PCCP

PAPER

View Article Online
View Journal | View Issue

Cite this: *Phys. Chem. Chem. Phys.*, 2018, **20**, 5200

A photoelectron spectroscopy and quantum chemical study on ternary Al–B–O clusters: $Al_nBO_2^-$ and Al_nBO_2 (n = 2, 3)†

Ting Ou,[a] Yuan Feng,[b] Wen-Juan Tian,[a] Li-Juan Zhao,[b] Xiang-Yu Kong,[b] Hong-Guang Xu,[b] Wei-Jun Zheng *[bc] and Hua-Jin Zhai *[a]

Received 20th December 2017,
Accepted 16th January 2018

DOI: 10.1039/c7cp08512e

rsc.li/pccp

Both B and Al have high oxygen affinity and their oxidation processes are highly exothermic, hinting at intriguing physical chemistry in ternary Al–B–O clusters. We report a combined photoelectron spectroscopy and density-functional study on the structural, electronic, and bonding properties of $Al_nBO_2^-$ and Al_nBO_2 (n = 2, 3) clusters. Ground-state vertical detachment energies (VDEs) are measured to be 2.83 and 2.24 eV for $Al_2BO_2^-$ and $Al_3BO_2^-$, respectively. A weak isomer is also observed for $Al_3BO_2^-$ with a VDE of 1.31 eV. Coalescence-kick global searches allow the identification of candidate structures, confirmed *via* comparisons with experiment. The $Al_2BO_2^-$ anion is V-shaped in geometry, C_s ($^1A'$), with an Al center connecting to OB and OAl terminals. It can be viewed alternatively as the fusion of BOAl and AlOAl by sharing an Al atom. $Al_3BO_2^-$ has a C_s ($^2A''$) global minimum in which an Al_2 dimer interacts with bridging boronyl (BO) and an OAl unit, as well as a low-lying C_{2v} ($^2B_2$) isomer consisting of boronyl and OAl that are doubly bridged by two Al atoms. The BO_2 block (linear O═B═O chain) is nonexistent in any of the anion and neutral species. Chemical bonding in these Al–B–O clusters is elucidated *via* canonical molecular orbitals and adaptive natural density partitioning. The cluster structures are also rationalized using the concept of sequential and competitive oxidation of B *versus* Al centers in Al_nB. The first O atom prefers to oxidize B and form BO, whereas the second O atom has options to interact with a fresh Al/Al_n/Al_nB unit or a BO group. The former route wins thermodynamically, leading to the observed geometries.

1. Introduction

For many years, researchers in the nanocluster community have devoted efforts to investigate the structural and electronic properties of Al–O and B–O mixed clusters. Among the Al–O clusters, multiple isomers[1,2] were observed in $Al_3O_3^-$ and $Al_4O_6^-$, the former undergoing photoisomerization.[1] Unconventional Al–O cluster structures were also revealed.[3] For B–O clusters, persistent interest since the 1950s primarily aims at understanding the combustion of boron and boranes and development of highly energetic boron-based propellants.[4] Renewed recent interest is focused on the nature of bonding in B–O clusters.[5–23] In particular, boronyl was discovered as a key concept that governs boron oxide clusters, from the gas phase to synthetic compounds.[10,24] Boronyl features a B≡O triple bond, reflecting strong oxygen affinity of boron. The robustness of boronyl alters or destroys multifold (π and σ) aromaticity in bare boron clusters,[25–37] which are intrinsically electron-deficient and possess intriguing bonding properties.

The Al and B elements are isovalent and both have high oxygen affinity. Al powder is known as fuel in solid propellants. It is thus natural to ask some fundamental questions: how does the oxidation of binary Al–B clusters proceed? What is the nature of bonding in ternary Al–B–O clusters? Since the BO_2^- cluster[11] is rather stable in the gas phase and BO_2, with an electron affinity (EA) of 4.46 eV, belongs to the class of species called superhalogens,[38] will Al–B–O_2 clusters maintain a BO_2 structural block? If not, why? The title $Al_nBO_2^-$ and Al_nBO_2 (n = 2, 3) clusters are the simplest species that should help address these questions and offer insight into bonding in the Al–B–O ternary system.

[a] *Nanocluster Laboratory, Institute of Molecular Science, Shanxi University, Taiyuan 030006, China. E-mail: hj.zhai@sxu.edu.cn*

[b] *Beijing National Laboratory for Molecular Sciences (BNLMS), State Key Laboratory of Molecular Reaction Dynamics, Institute of Chemistry, Chinese Academy of Sciences, Beijing 100190, China. E-mail: zhengwj@iccas.ac.cn*

[c] *University of Chinese Academy of Sciences, Beijing 100049, China*

† Electronic supplementary information (ESI) available: Alternative optimized structures of $Al_nBO_2^-$ and Al_nBO_2 (n = 2, 3) clusters at the B3LYP/6-311+G(d) level (Fig. S1–S4); a comparison of simulated photoelectron spectra of $Al_3BO_2^-$ based on isomers **3b**/**3c** with experimental data (Fig. S5); and CMOs and AdNDP bonding elements for isomers **2a**/**2b**/**3a**/**3d** (Fig. S6–S9). See DOI: 10.1039/c7cp08512e

To our knowledge, there have been few prior studies on the Al–B–O clusters, except for computational work on $Al(BO_2)_n$ and $Al(BO_2)_n^-$ (n = 1–4).[39] Therefore, only selected works with respect to Al–O, B–O, and TM–BO_2 (TM = transition metal) clusters are discussed below. The AlO dimer has a bond distance of ~1.6 Å and a bond energy of 512 kJ mol^{-1} (122.4 kcal mol^{-1}), compared to ~1.2 Å and 806 kJ mol^{-1} (192.6 kcal mol^{-1}) for boronyl (BO).[10] While these values differ, both Al–O and B–O bonds are quite strong. In terms of bonding nature, the Al–O bond is more ionic. Boronyl as a new ligand (comparable to CO or CN) was demonstrated in an array of experimental and computational studies lately,[10,24] in which it occurs in a terminal, bridging, or capping fashion and maintains chemical integrity. Boronyl is a monovalent σ radical, facilitating BO/Au/H isolobal analogy. The EAs of AlO/AlO_2 and BO/BO_2 were measured to be similar *via* photoelectron (PE) spectroscopy,[11,40] and AlO_2 and BO_2 were classified as superhalogens with EAs of 4.23 and 4.46 eV, respectively. BO_2^- was also observed in matrix isolation infrared spectroscopy.[5] Chemical bonding in heterocyclic B–O clusters was explored as well. A D_{3h} B_6O_6 cluster[16] with a boroxol (B_3O_3) core was shown as an analog of benzene or boroxine. A rhombic B_2O_2 ring in B–O clusters features four-center four-electron (4c–4e) π bond, that is, the "o-bond",[19,21] which is an extension of the hypervalent 3c–4e bond in linear XeF_2 species.

BO and BO_2 clusters can be used to form transition metal complexes. Auro-boron oxide clusters Au_nBO^- (n = 1–3) were studied using PE spectroscopy,[41] which contain boronyl and exhibit spectral patterns similar to those of Au_nH^-.[42] A number of studies were reported on M–BO_2 (M = Cu, Ag, Au, Fe, Mn) complex clusters,[43–49] showing that a BO_2 block retains in the complexes. The EAs of $Cu(BO_2)_2$ and $Au(BO_2)_2$ were measured to be 5.07 and 5.70 eV, respectively, from PE spectroscopy,[44,49] whereas $Fe(BO_2)_2$ and $Mn(BO_2)_2$ have EAs as high as 6.9 eV according to a computational study.[46] These EA values are greater than that of superhalogen BO_2 cluster (4.46 eV),[11] suggesting the formation of hyperhalogens.[49]

In this contribution, we report a PE spectroscopy and density-functional theory (DFT) study on $Al_nBO_2^-$ and Al_nBO_2 (n = 2, 3) clusters. The combined experimental and computational data establish their global minimum (GM) and lowest-lying isomeric structures. Bonding analyses indicate the presence of boronyl, multifold three-center two-electron (3c–2e) Al–O–Al and Al–O–B π/σ bonds, π and σ aromaticity for the Al_2B ring, and 3c–2e π/σ bonds for the rhombic BAl_2O ring. In contrast to the M–BO_2 (M = Cu–Au, Fe, Mn) clusters in previous reports,[43–49] a BO_2 unit (that is, linear O═B═O chain) does not exist in $Al_nBO_2^-$ and Al_nBO_2 (n = 2, 3). We propose a concept of sequential and competitive oxidation of B *versus* Al centers in binary Al–B clusters, which holds the key to understanding ternary Al–B–O clusters.

2. Methods

2.1. Photoelectron spectroscopy

The experiments were carried out on a home-built PE spectroscopy apparatus[50] consisting of a laser vaporization source, a time-of-flight mass spectrometer, and a magnetic-bottle PE spectrometer. Briefly, $Al_nBO_2^-$ (n = 2, 3) anion clusters were generated from an Al/B mixed target (Al/B molar ratio 60 : 1), using the second harmonic of an Nd:YAG laser (Continuum Surelite II-10). Residual oxygen in vacuum or from the target serves as the oxygen source for Al–B–O clusters. Typical laser power for vaporization was 10 mJ per pulse. A helium carrier gas with 4 atm backing pressure was injected from a pulsed valve (General Valve Series 9) for cluster growth and cooling *via* supersonic expansion. Each cluster species was mass selected, decelerated, and crossed with another Nd:YAG laser (355 and 266 nm) for photodetachment. Photoelectrons were collected and analyzed using the magnetic-bottle PE spectrometer, calibrated using the known spectra of Cu^- and Au^-. Energy resolution of the apparatus was ~40 meV for electrons of 1 eV kinetic energy.

2.2. Computational methods

GM searches for the Al–B–O clusters were accomplished using the Coalescence Kick (CK) method,[51–53] aided with manual structural constructions. CK searches were done at the hybrid B3LYP level[54,55] with a small basis set of 3-21G. A total of 2600 stationary points were probed on the potential energy surface for $Al_2BO_2^-$; those for Al_2BO_2, $Al_3BO_2^-$, and Al_3BO_2 were 2600, 3000, and 3000, respectively. Candidate low-lying structures were fully re-optimized at the B3LYP/6-311+G(d) level. Frequency calculations were performed at the same level to ensure that all reported structures are true minima. Single-point CCSD(T) calculations[56–59] were done at the B3LYP geometries to benchmark relative energies for top isomers.

Adiabatic and vertical detachment energies (ADEs and VDEs) for low-lying anion isomers were calculated at B3LYP for the ground state and at time-dependent B3LYP (TD-B3LYP)[60,61] for the excited states, based on which simulated PE spectra were produced. Bonding analyses were performed *via* canonical molecular orbitals (CMOs) and adaptive natural density partitioning (AdNDP).[62] Natural bond orbital (NBO) analyses[63] were carried out to obtain natural atomic charges. Orbital compositions were analyzed using Multiwfn.[64] AdNDP calculations were accomplished using the AdNDP program. Other calculations were done using Gaussian 09.[65]

3. Experimental results

The PE spectra of $Al_2BO_2^-$ and $Al_3BO_2^-$ were recorded at 355 nm (3.496 eV) and 266 nm (4.661 eV); see Fig. 1 and 2. The measured ADEs and VDEs are listed in Table 1, as compared to computational data at B3LYP based on candidate low-lying structures. The PE bands are labeled as X, X′, and A–C. Band X is the transition from an anion ground-state to that of the neutral, and X′ represents a minor isomer. Bands A–C are transitions to the excited states of the neutral. All reported ADEs and VDEs have an experimental uncertainty of ±0.08 eV.

The $Al_2BO_2^-$ cluster shows two PE bands: X and A (Fig. 1(a) and (b)). The ground-state VDE is measured from the peak

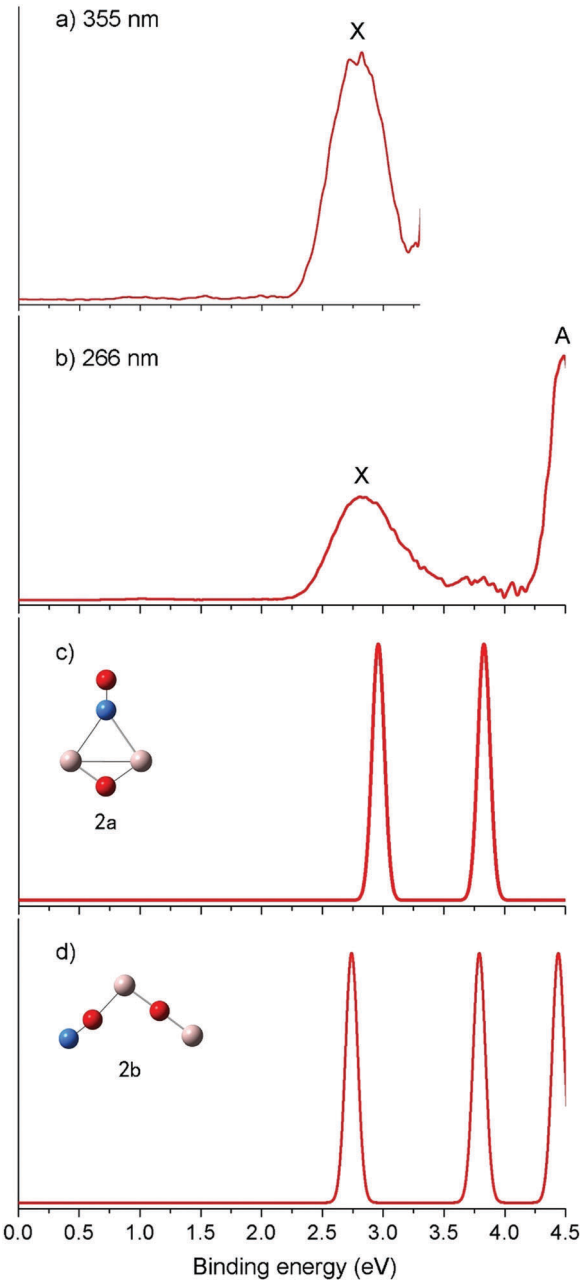

Fig. 1 Experimental photoelectron (PE) spectra of the $Al_2BO_2^-$ cluster taken at (a) 355 nm (3.496 eV) and (b) 266 nm (4.661 eV), as compared to those simulated on the basis of isomers (c) **2a** (C_{2v}, $^1A_1$) and (d) **2b** (C_s, $^1A'$). The simulations were done at the time-dependent B3LYP/6-311+G(d) (TD-B3LYP) level, by fitting calculated vertical detachment energies (VDEs) with unit-area Gaussian functions. Structure **2b** is responsible for the experimental PE spectra (see text).

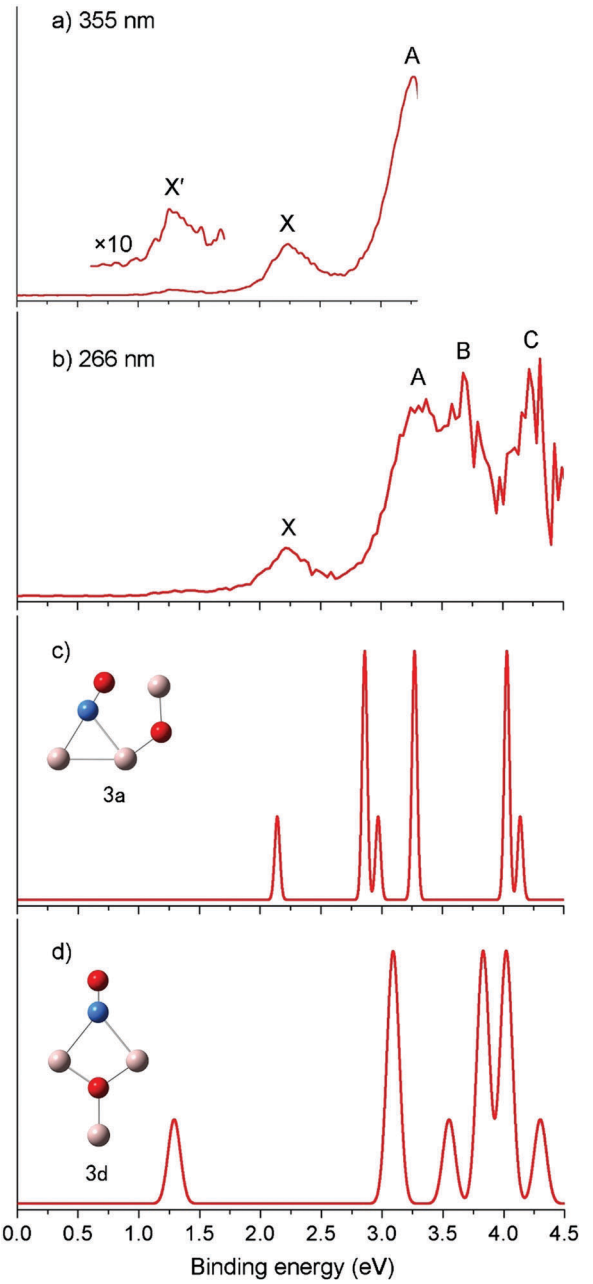

Fig. 2 Experimental PE spectra of $Al_3BO_2^-$ cluster taken at (a) 355 and (b) 266 nm, as compared to those simulated on the basis of isomers (c) **3a** (C_s, $^2A''$) and (d) **3d** (C_{2v}, $^2B_2$). The simulations were done at the TD-B3LYP level, by fitting calculated VDEs with unit-area Gaussian functions. Simulated PE spectra of **3b** and **3c** are shown in the ESI.†

maximum of X to be 2.83 eV, whereas its well-defined onset allows an estimate of ADE (2.39 eV). Band A is located at beyond 4.3 eV and only its leading portion is accessible at 266 nm. A rough VDE of ~4.5 eV is estimated for band A. A secondary feature (3.75 eV) appears in between X and A, likely due to a shake-up transition (that is, a two-electron process of kicking out one electron from an anion and simultaneously promoting a second electron to an upper level).

$Al_3BO_2^-$ exhibits a complicated spectral pattern (Fig. 2(a) and (b)). Band X is well defined, yielding a VDE of 2.24 eV and an ADE of 1.93 eV. Excited states A–C are located at 3.30, 3.67, and ~4.2 eV, respectively, which are more intense than X, consistent with an open-shell anion cluster. Spikes in bands B and C are due to a low signal-to-noise ratio in that regime. On the low binding energy side, there is band X′, being less than 10% the intensity of X. Band X′ is attributed to a coexisting anion isomer (VDE: 1.31 eV; ADE: 1.14 eV).

Table 1 Adiabatic and vertical detachment energies (ADEs and VDEs) from photoelectron (PE) spectra of $Al_2BO_2^-$ and $Al_3BO_2^-$, compared to those calculated at the B3LYP level

Species	Feature	VDE/ADE (exptl)[a]	Isomer 1[b]	VDE/ADE (theo)[a,c]	Isomer 2[b]	VDE/ADE (theo)[a,c]
$Al_2BO_2^-$	X	2.83/*2.39*	**2a** ($^2A_1$)	2.95/*1.90*	**2b** ($^2A'$)[d]	2.73/*2.30*
	A	~4.5[e]	($^2B_2$)	3.82	($^2A'$)	3.76
$Al_3BO_2^-$	X	2.24/*1.93*	**3a** ($^1A'$)	2.13/*1.68*		
	A	3.30	($^3A''$)	2.85		
	B	3.67	($^3A''$)	3.26		
	C	~4.2	($^3A''$)	4.02		
	X′	1.31/*1.14*			**3d** ($^1A_1$)	1.28/*1.15*

[a] All energies are given in eV, with an experimental uncertainty of ±0.08 eV. Ground-state ADEs are shown in italic, which represent electron affinities of the corresponding neutral clusters. [b] Anion PE spectroscopy probes the ground state and excited states of the neutral species. Anion isomeric structures are denoted in bold (**2a**, **2b**, **3a**, and **3d**) and final states are shown in parentheses. [c] VDE/ADE for the ground state at the B3LYP/6-311+G(d) level and VDEs for excited states at time-dependent B3LYP (TD-B3LYP). [d] **2b** is assigned as the carrier for experimental PE spectra of $Al_2BO_2^-$; see text. [e] Estimated value from band A, which is partially accessed at 266 nm.

4. Theoretical results

4.1. $Al_2BO_2^-$ and Al_2BO_2 clusters

Low-lying structures of $Al_2BO_2^-$ are presented in Fig. 3 (see also Fig. S1, ESI†), and those of the Al_2BO_2 neutral are presented Fig. 4 and Fig. S2 (ESI†). For the anion, the lowest two isomers, kite-like **2a** (C_{2v}, $^1A_1$) *versus* V-shaped **2b** (C_s, $^1A'$), are within 0.70 kcal mol^{-1} at the B3LYP level (Fig. 3). As a note, here and throughout the text, **2** or **3** denotes the number of Al atoms in a cluster and **a**/**b**/**c**/**d** the energy order of an isomer. Isomers **2a**/**2b** reverse in energy at single-point CCSD(T), with the latter being marginally more stable by 0.16 kcal mol^{-1}. Other isomers are at least 2 kcal mol^{-1} higher in energy. Therefore, **2a** and **2b** are isoenergetic and computationally indistinguishable; both should be considered as candidates for the PE spectra.

The potential energy surface of the Al_2BO_2 neutral seems to be more complex. Top three isomers are crucial (Fig. 4): **2a**′ (C_s, $^2A'$), **2b**′ (C_{2v}, $^2A_1$), and **2c**′ (C_s, $^2A'$). Isomers **2a**′/**2b**′ are within 0.41 kcal mol^{-1} at B3LYP and **2a**′/**2c**′ within 0.58 kcal mol^{-1} at single-point CCSD(T). These three isomers are either zig-zag or V-shaped. Interestingly, upon electron removal, the kite-like **2a** anion undergoes structural transformation directly to V-shaped neutral **2c**′. The kite-like structure similar to the **2a** anion is not a minimum for the neutral. Additional neutral isomers are at least 2 kcal mol^{-1} higher in energy.

4.2. $Al_3BO_2^-$ and Al_3BO_2 clusters

As shown in Fig. 3 (see also Fig. S3, ESI†), two low-lying isomers **3a** (C_s, $^2A''$) and **3b** (C_s, $^2A''$) are identified for $Al_3BO_2^-$, which are within 0.48 kcal mol^{-1} at the B3LYP level. However, **3b** becomes 2.24 kcal mol^{-1} higher in energy at single-point CCSD(T). Thus, **3a** can be claimed as the GM of the system. Both **3a**/**3b** have an Al_2 core that interacts with terminal OAl and bridging BO groups. They differ only in the orientation of the terminal OAl unit, which bends to the BO group in **3a** so as to gain additional Al2–O4 bonding (Fig. 3(b)). Indeed, the Al2–O4 distance shrinks markedly from 5.33 Å in **3b** to 2.13 Å in **3a**.

The neutral Al_3BO_2 cluster has a well-defined GM: **3a**′ (C_{2v}, $^1A_1$) (Fig. S4, ESI†). Alternative isomers are not competitive. Structure **3a**′ consists of an Al_2 dimer interacting with BO and OAl, forming a rhombic BAl_2O ring. Alternatively, it can be viewed as the fusion of Al_3O and BO. The BO group is boronyl in nature. Its corresponding anion ranks only as the fourth isomer, **3d** (C_{2v}, $^2B_2$), being ~3 kcal mol^{-1} above GM **3a**.

4.3. Bond distances in $Al_nBO_2^-$ and Al_nBO_2 (n = 2, 3) clusters

A survey of Al–Al, Al–B, Al–O, and B–O distances in key structures of $Al_nBO_2^-$ and Al_nBO_2 (n = 2, 3) offers insight into bonding in the systems (Fig. 3 and 4). As a reference, the B–O single bond has an upper bound of 1.48 Å,[66] whereas B=O and B≡O bonds are typically 1.28 and 1.21 Å,[10] respectively. Al–Al, Al–B, Al–O, and Al=O bonds are around 2.5, 2.1, 1.9, and 1.7 Å, respectively.[66] Using these values, one can see that boronyl dominates **2a**/**3d**/**2c**′/**3a**′ (1.21–1.23 Å). Additional robust B–O

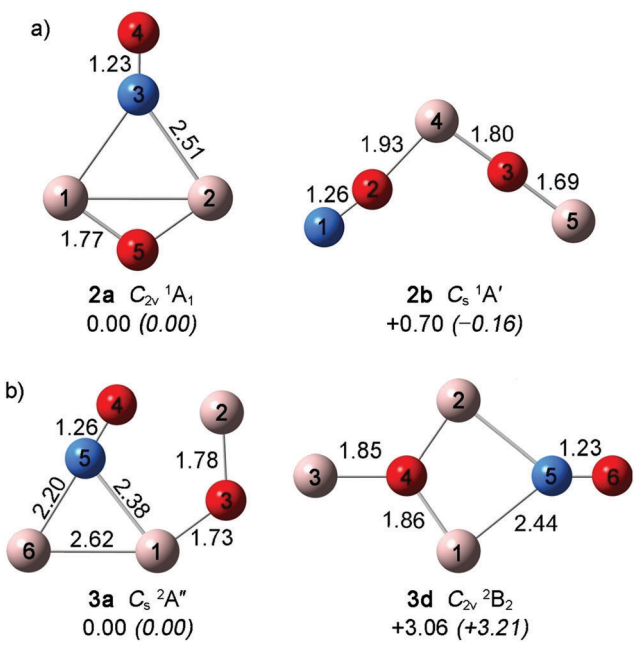

Fig. 3 Optimized top low-lying structures of $Al_2BO_2^-$ and $Al_3BO_2^-$ anion clusters at the B3LYP/6-311+G(d) level. (a) $Al_2BO_2^-$ **2a** (C_{2v}, $^1A_1$) and $Al_2BO_2^-$ **2b** (C_s, $^1A'$). (b) $Al_3BO_2^-$ **3a** (C_s, $^2A''$) and $Al_3BO_2^-$ **3d** (C_{2v}, $^2B_2$). Relative energies are indicated in kcal mol^{-1} at B3LYP/6-311+G(d) and single-point CCSD(T)//B3LYP/6-311+G(d) (in parentheses) levels. Bond distances are shown in angstroms. The B atom is in blue, Al in pink, and O in red.

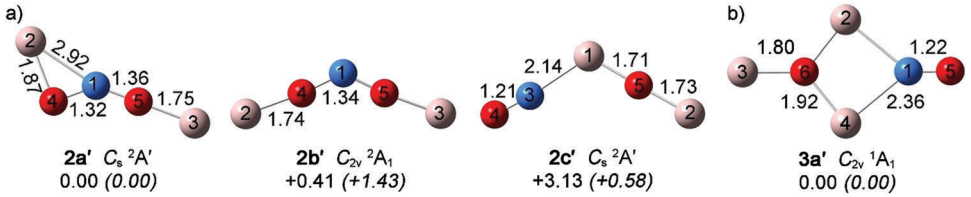

Fig. 4 Optimized top low-lying structures of Al_2BO_2 and Al_3BO_2 neutral clusters at the B3LYP/6-311+G(d) level. (a) **2a**′ (C_s, ^{2}A′), **2b**′ (C_{2v}, ^{2}A$_1$), and **2c**′ (C_s, ^{2}A′) of Al_2BO_2. (b) **3a**′ (C_{2v}, ^{1}A$_1$) of Al_3BO_2. Relative energies are indicated in kcal mol^{-1} at B3LYP/6-311+G(d) and single-point CCSD(T)//B3LYP/6-311+G(d) (in parentheses) levels. Bond distances are shown in angstroms. The B atom is in blue, Al in pink, and O in red.

bonds are present in **2b**/**3a** (1.26 Å, beyond double bond), as well as **2a**′ and **2b**′ (1.32/1.36 and 1.34 Å, probably beyond a single bond). A typical Al–O single bond exists only in **3a**′ (1.80 Å), whereas an Al–B single bond is present in **2c**′ (2.14 Å). For other Al–O bonds, those in **2b** (1.69 Å), **3a** (1.73 Å), **2a**′ (1.75 Å), **2b**′ (1.74 Å), and **2c**′ (1.71/1.73 Å) are likely beyond single bond. Interestingly, despite the lack of a "bond", the Al2–O4 distance in **3a** (2.13 Å) shows discernible bonding interaction, which helps stabilize **3a** as the GM.

5. Discussion

5.1. Comparison between experiment and theory

We have established energetically in Section 4 that isomers **2a**/**2b** are candidate structures for the $Al_2BO_2^-$ anion cluster, whereas **3a** is clearly the GM of $Al_3BO_2^-$. Simulated PE spectra using **2a**/**2b** and **3a**/**3d** are shown in Fig. 1 and 2, respectively; those of **3b**/**3c** deviate substantially from experiment and are presented in Fig. S5 (ESI†). Both **2a** and **2b** match experiment for the position of band X (and qualitatively for the X–A gap), although the first excited-state appears to be underestimated by ~0.7 eV at TD-B3LYP (Table 1). Thus, with regard to TD-B3LYP data and simulated PE spectra, only the overall PE pattern is important for comparison with experiment.

For the ground-state transition, a quantitative comparison is possible between experiment and theory, the latter being done at the B3LYP level. It appears to be the norm that B3LYP slightly underestimates ADE/VDE, for three out of four species (**2b**/**3a**/**3d**) listed in Table 1. Specifically, calculated ADE/VDE are 1.90/2.95 eV for **2a** *versus* 2.30/2.73 eV for **2b**, which are compared to the experimental values of 2.39/2.83 eV. Structure **2b** shows quantitative agreement with experiment (errors: 0.09–0.10 eV). The calculated VDE of **2a** is also in reasonable agreement with experiment and yet biased to the opposite direction. Fortunately, the calculated ADE of **2a** underestimates experimental data by as large as 0.49 eV, which is substantial in particular considering the fact that the same calculation overestimates VDE by 0.12 eV.

The above fatal discrepancy helps distinguish between **2a** and **2b**, despite their computational complexity in terms of energetics (Fig. 3). The primary reason is that the structure associated with **2a** is not a minimum for the neutral (see Section 4.1). Upon photodetachment **2a** undergoes substantial structural changes to reach neutral isomer **2c**′ (Fig. 4). This effect can be quantified using the so-called "reorganization energy" (ROE), defined as the difference between ADE and VDE of a specific transition. The calculated ROE for **2a** amounts to 1.05 eV, suggesting an extremely broad PE band, which is in disagreement with band X (experimental ROE: 0.44 eV). In contrast, **2b** has a calculated ROE of 0.43 eV. Therefore, we shall conclude that **2b** (rather than **2a**) is the genuine carrier of experimental PE spectra.

Assignment of the PE spectra of $Al_3BO_2^-$ is simple and straightforward. The global minimum **3a** is responsible for main bands X and A–C. The first few VDEs of **3a** are calculated to be 2.13, 2.85, 3.26, and 4.02 eV, which show an overall pattern perfectly in line with experiment. Quantitatively, the measured VDEs are 2.24, 3.30, 3.67, and ~4.2 eV, respectively, and again the excited states are underestimated in TD-B3LYP (by 0.18–0.45 eV). Also, the ground-state VDE is underestimated by 0.11 eV at B3LYP, which is normal as stated above.

The weak isomer X′ of $Al_3BO_2^-$ is assigned to **3d**, which has the calculated ADE/VDE of 1.15/1.28 eV, in excellent agreement with experiment (1.14/1.31 eV). Two alternative isomers **3b** and **3c** are energetically in between **3a** and **3d** (Fig. S3, ESI†). However, **3b** and **3c** do not fit the labeled PE bands (X′, X, and A–C) and they can be ruled out as a carrier of these bands; see Fig. S5 (ESI†).[67] It is stressed that **3d** has a sizable energy gap of 1.82 eV and extremely low ADE/VDE (Fig. 2(d)), which indicate an electronically robust neutral cluster. Indeed, while **3d** as an anion occurs only as a minor isomer, its corresponding neutral **3a**′ is clearly the GM (Fig. S4, ESI†).

5.2. Chemical bonding

Generally, the bonding in Al–B–O clusters is of mixed covalent and ionic characters, the latter originating from the polar nature of B–O and Al–O interactions due to their difference in electronegativity (1.61 for Al, 2.04 for B, and 3.44 for O). Natural charges from NBO analyses are shown in Fig. 5 for $Al_nBO_2^-$ and Al_nBO_2 (n = 2, 3). The charge on an O center depends on its coordination environment, which is sorted to three categories. Category 1 is terminal O (bonded solely to B), with a charge of −0.8 to −1.1 $|e|$. In category 2, an O center is inserted in between two atoms or bridges them. For the AlB case O has a charge of −1.2 to −1.3 $|e|$ and for the Al_2 case −1.5 to −1.6 $|e|$. Category 3 is an O center inserted in Al_3, in which O carries a charge of −1.7 $|e|$. The negative charges are provided by neighboring B/Al atoms (and not due to the extra charge of an anion). Electron redistributions in these ternary clusters are primarily local processes.

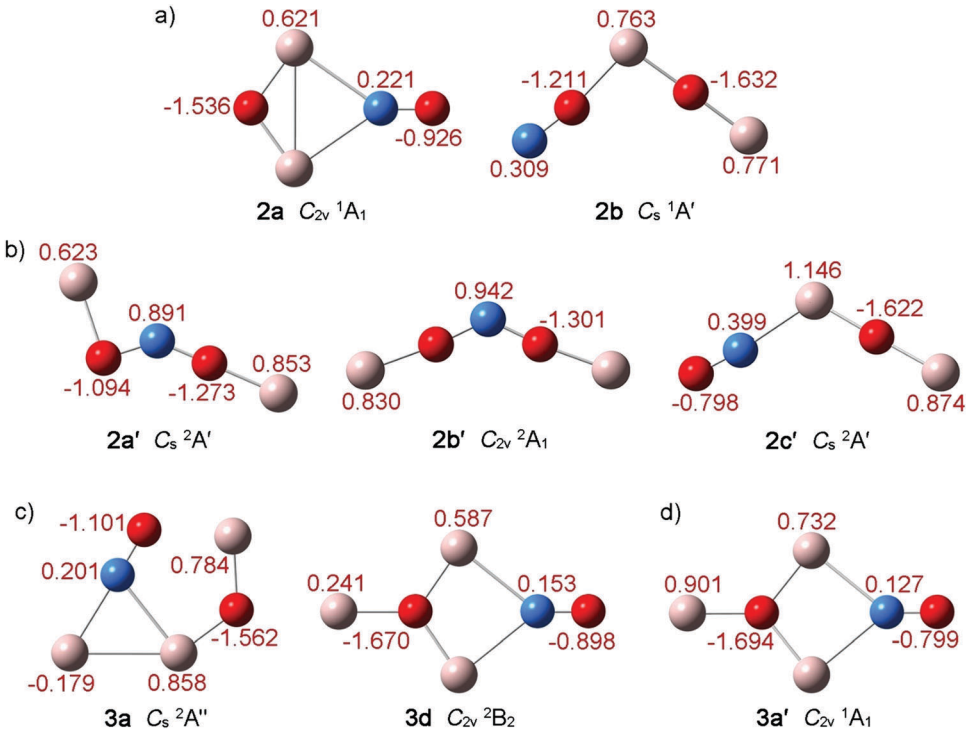

Fig. 5 Natural atomic charges for selected isomeric structures. (a) **2a** and **2b** of $Al_2BO_2^-$. (b) **2a′**, **2b′**, and **2c′** of Al_2BO_2. (c) **3a** and **3d** of $Al_3BO_2^-$. (d) **3a′** of Al_3BO_2.

The essence of bonding in the clusters can be obtained from CMO analyses in combination with orbital component data, species by species, which are too tedious to describe here. Bonding pictures thus achieved are compared to bond distances described in Section 4.3. Furthermore, the bonding patterns are confirmed *via* AdNDP analyses.[68] Selected CMOs and AdNDP bonds are presented in Fig. 6 and 7 for structures **2a**, **2b**, **3a**, and **3d**, and the occupation numbers (ONs) are remarkably close to ideal (ON = 2.00 $|e|$). Full sets of CMOs and AdNDP data for **2a**/**2b**/**3a**/**3d** are presented in Fig. S6–S9 (ESI†). All bonding data are highly concerted from the CMOs, orbital component analyses, bond distances, and AdNDP, which lead to the proposed Lewis structures for the species. We comment that both **2a**/**2b** can be viewed as the fusion of BO and Al_2O, except that the orientation of BO flips by 180° so that it becomes OB in **2b**; the repulsion between two O centers in the latter eventually leads to an open V-shaped structure. Likewise, **3a**/**3d** are both composed of Al_2, BO, and OAl, differing only in the orientation of OAl. With such simple reorganizations, the nature of bonding changes fundamentally, which is intriguing.

We now briefly discuss the crucial bonding features (Fig. 8 and 9). First of all, we state that, contrary to anticipation, classical Lewis 2c–2e bonds are rare rather than routine in these Al–B–O clusters. Second, multifold B–O bonding dominates all structures. It appears as terminal boronyl (B≡O), bridging boronyl, terminal OB, and an OBO unit, which have the B–O bond order of three (**2a**, **3a**, **2c′**), three (**3d**, **3a′**), beyond two (**2b**), and three-fold (**2a′**, **2b′**), respectively. Third, multifold

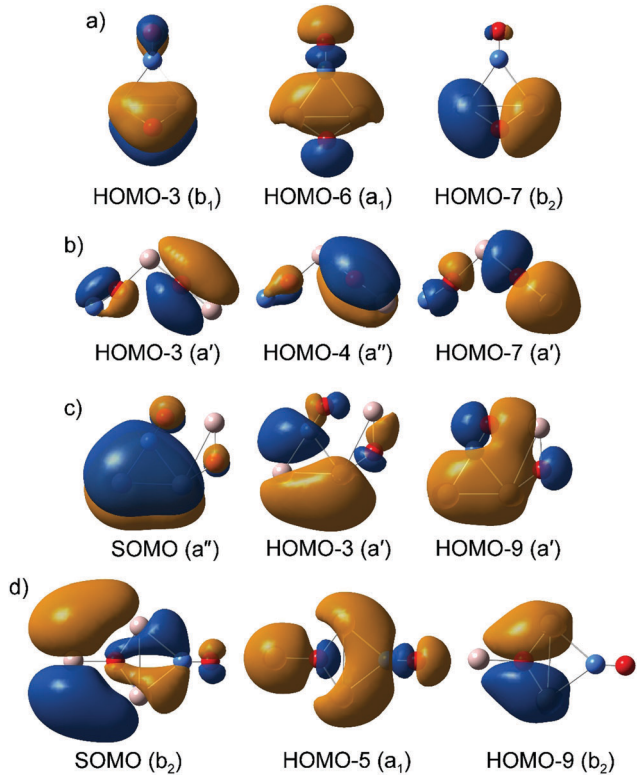

Fig. 6 Selected canonical molecular orbitals (CMOs) of (a) $Al_2BO_2^-$ (**2a**), (b) $Al_2BO_2^-$ (**2b**), (c) $Al_3BO_2^-$ (**3a**), and (d) $Al_3BO_2^-$ (**3d**). SOMO stands for a singly occupied molecular orbital.

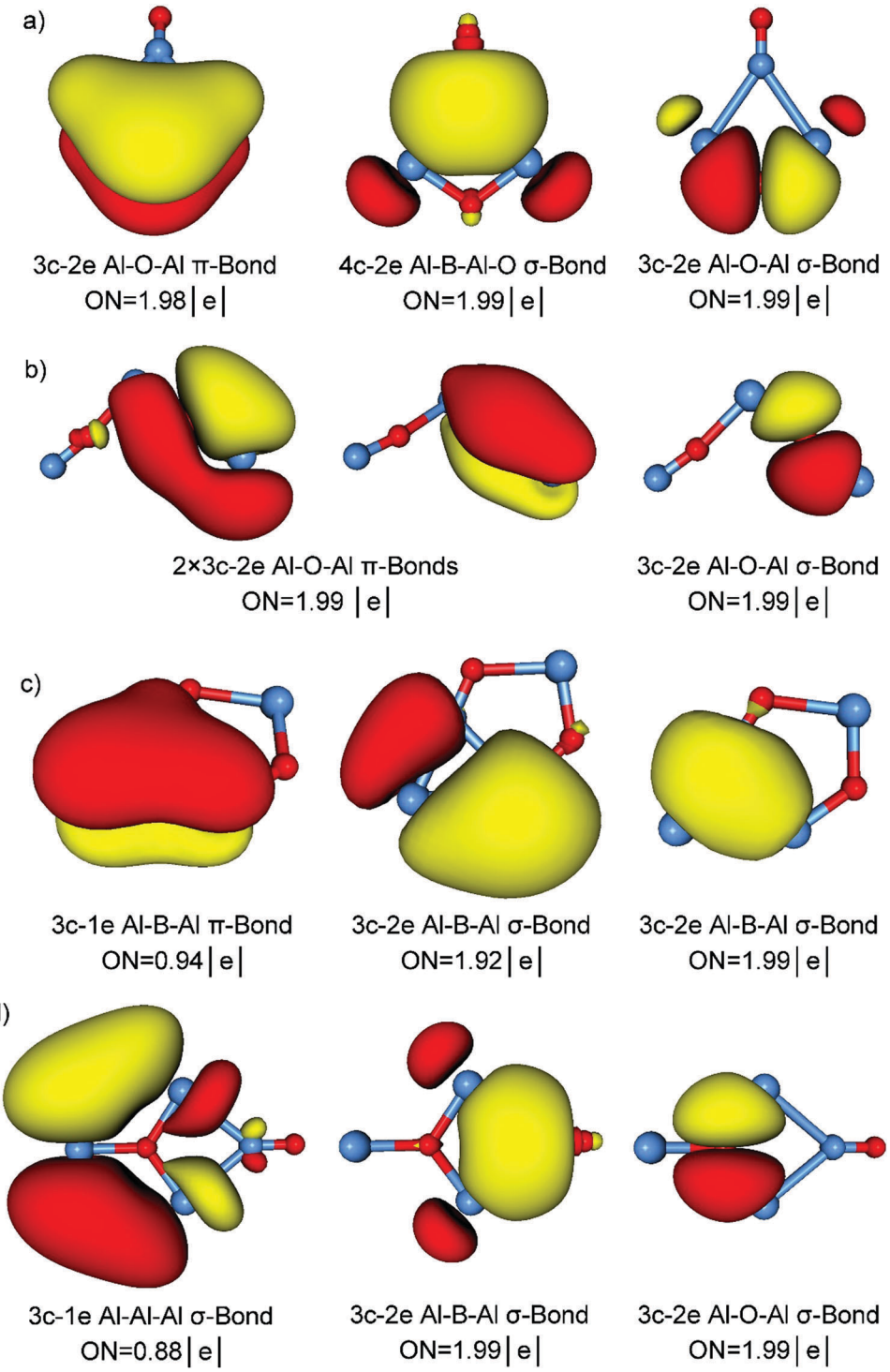

Fig. 7 Selected delocalized AdNDP bonds for (a) $Al_2BO_2^-$ (**2a**), (b) $Al_2BO_2^-$ (**2b**), (c) $Al_3BO_2^-$ (**3a**), and (d) $Al_3BO_2^-$ (**3d**), which correspond to the CMOs depicted in Fig. 6. Occupation numbers (ONs) are shown.

Al–O bonding is present in five out of eight species, in the form of Al–O–Al (**2b**, **3a**, **2c′**) or Al–O–B (**2a′**, **2b′**) bonds; see also Fig. 6(b). These 3c–2e σ/π bonds are uneven for the two ends, even in the case of **2b** (1.80 *versus* 1.69 Å), reflecting the polar nature of Al–O and B–O bonding. Remarkably, four out of six bonds in **2b** and all six bonds in **2b′** are 3c–2e in nature, and the linear or quasi-linear Al–O–Al unit in **2b**/**3a**/**2c′** is entirely held together by 3c–2e bonds. Fourth, the majority of Al centers each have a lone-pair, despite the electron-deficiency for Al–B–O clusters. Fifth, a triangular Al_2B unit in **3a** possesses 3c–2e σ and 3c–1e π bonds (see also Fig. 6(c)), rendering the species (π and σ) double aromaticity. In contrast, a rhombic BAl_2O ring

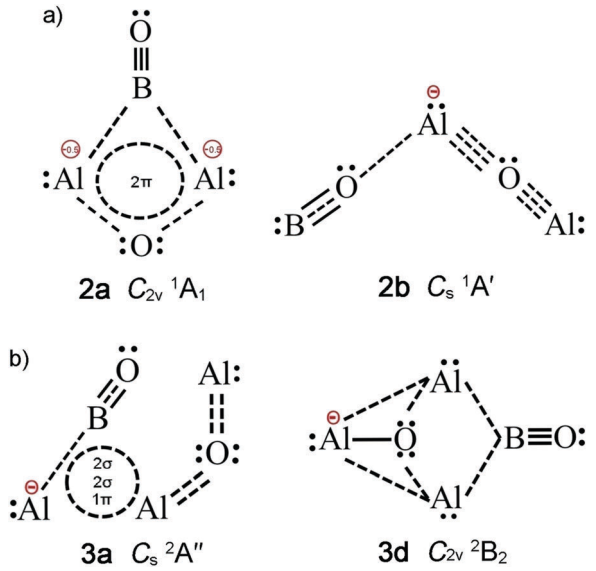

Fig. 8 Approximate Lewis presentations of (a) $Al_2BO_2^-$ (**2a**) and $Al_2BO_2^-$ (**2b**) and (b) $Al_3BO_2^-$ (**3a**) and $Al_3BO_2^-$ (**3d**). The location of an extra electron in the anion is indicated in red color. The solid line represents a two-center two-electron (2c–2e) bond. The dashed line or circle denotes a delocalized bond (including linear 3c–2e bond).

in **2a**/**3d**/**3a**′ is held together by 3c–2e BAl_2 and Al_2O σ bonds, as well as a delocalized Al_2O π bond in **2a** (Fig. 6(a) and (d)). Lastly, the mysterious Al2–O4 interaction in **3a** is traced to a number of CMOs, such as HOMO−8 through HOMO−10 (Fig. S8, ESI†), which collectively result in a NBO bond order of 0.15.

5.3. Competitive oxidation of B *versus* Al centers in ternary Al–B–O clusters

An alternative way to rationalize the cluster structures of $Al_nBO_2^-$ and Al_nBO_2 (n = 2, 3) is the sequential and competitive oxidation of binary Al_nB^- and Al_nB clusters by two O atoms. Intuitively, initial oxidation occurs at the B site, because it is more electronegative and favorable for the formation of boronyl, which is known to govern the geometries of boron oxide clusters.[10] Indeed, BO, OB, and OBO units dominate ternary Al–B–O clusters (Fig. 8 and 9).

When the first O atom is incorporated into Al_nB^- and Al_nB, the second O atom has two options. Option 1 is to further attack the B center to reach BO_2, which is also highly exothermic. Option 2 is to explore an uncharted territory (Al, Al_n, or Al_nB). The two processes compete with each other and thermodynamics dictates which route wins. A simple calculation at B3LYP indicates that conversion of BO to BO_2 thermodynamically gains 131.3 kcal mol^{-1}. On the other hand, oxidation of Al or Al_n/Al_nB by an O atom is highly exothermic as well. For example, an energy gain of 122.3 kcal mol^{-1} is achievable to form AlO.[10] Of course, these numbers shall serve as a rough reference only, because bonding in Al–B–O clusters is far more complex than that in isolated BO, BO_2, or AlO species. Nevertheless, in ternary Al–B–O clusters, oxidation of an Al center can become favorable in the second step, once a B center is oxidized to BO in the first step. Note that here we are comparing a partially oxidized B center and a fresh Al/Al_n/Al_nB unit. This concept rationalizes why $Al_2BO_2^-$ and $Al_3BO_2^-$ clusters all have a BO group, as well as Al-based Al_2O or Al_3O units (Fig. 8). Similar arguments apply for the TM–BO_2 (TM = Cu, Ag, Au) clusters in the literature.[44,45,47–49] The only difference is that oxidation of Cu/Ag/Au is less exothermic, which is not competitive with the conversion of BO to BO_2. Consequently, thermodynamics governs the formation of a BO_2 unit in $Cu(BO_2)^-$ and $Au(BO_2)^-$ clusters.[44,49]

6. Conclusions

We report a photoelectron (PE) spectroscopy and quantum chemical study on the structural and electronic properties and chemical bonding in ternary Al–B–O clusters: $Al_nBO_2^-$ and Al_nBO_2 (n = 2, 3). Global minimum and lowest-lying isomeric structures are identified *via* computer Coalescence Kick searches. Comparisons between experimental adiabatic and vertical detachment energies (ADEs and VDEs) with those calculated at B3LYP and time-dependent B3LYP (TD-B3LYP) levels allow the assignments of anion cluster structures. Bonding analyses of the Al–B–O clusters reveal boronyls, multifold Al–O–Al and Al–O–B σ/π bonds, a triangular Al_2B ring with π and σ aromaticity, and a rhombic BAl_2O ring with three-center two-electron (3c–2e) σ bonds. A BO_2 group is not present in these clusters, which can be rationalized using the concept of competitive oxidation of B *versus* Al centers.

Conflicts of interest

There are no conflicts to declare.

Acknowledgements

This work was supported by the National Natural Science Foundation of China (21573138) and the Chinese Academy of Sciences (Grant No. QYZDB-SSW-SLH024). H. J. Z. also gratefully acknowledges support from the Sanjin Scholar Distinguished Professors Program.

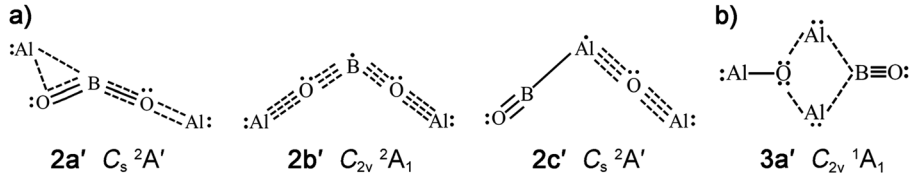

Fig. 9 Approximate Lewis presentations of **2a**′, **2b**′, and **2c**′ of Al_2BO_2, as well as **3a**′ of Al_3BO_2. Solid line represents a 2c–2e bond. Dashed line denotes the 3c–2e bond (linear or V-shaped) and the 2c–1e half bond.

References

1 H. Wu, X. Li, X. B. Wang, C. F. Ding and L. S. Wang, *J. Chem. Phys.*, 1998, **109**, 449.
2 M. Sierka, J. Döbler, J. Sauer, H. J. Zhai and L. S. Wang, *ChemPhysChem*, 2009, **10**, 2410.
3 M. Sierka, J. Döbler, J. Sauer, G. Santambrogio, M. Brümmer, L. Wöste, E. Janssens, G. Meijer and K. R. Asmis, *Angew. Chem., Int. Ed.*, 2007, **46**, 3372.
4 S. H. Bauer, *Chem. Rev.*, 1996, **96**, 1907.
5 T. R. Burkholder and L. Andrews, *J. Chem. Phys.*, 1991, **95**, 8697.
6 D. Peiris, A. Lapicki, S. L. Anderson, R. Napora, D. Linder and M. Page, *J. Phys. Chem. A*, 1997, **101**, 9935.
7 M. L. Drummond, V. Meunier and B. G. Sumpter, *J. Phys. Chem. A*, 2007, **111**, 6539.
8 M. T. Nguyen, M. H. Matus, V. T. Ngan, D. J. Grant and D. A. Dixon, *J. Phys. Chem. A*, 2009, **113**, 4895.
9 Z. Zhang, L. Pu, Q. S. Li and R. B. King, *Inorg. Chem.*, 2015, **54**, 2910.
10 H. J. Zhai, Q. Chen, H. Bai, S. D. Li and L. S. Wang, *Acc. Chem. Res.*, 2014, **47**, 2435.
11 H. J. Zhai, L. M. Wang, S. D. Li and L. S. Wang, *J. Phys. Chem. A*, 2007, **111**, 1030.
12 H. J. Zhai, S. D. Li and L. S. Wang, *J. Am. Chem. Soc.*, 2007, **129**, 9254.
13 S. D. Li, H. J. Zhai and L. S. Wang, *J. Am. Chem. Soc.*, 2008, **130**, 2573.
14 H. J. Zhai, C. Q. Miao, S. D. Li and L. S. Wang, *J. Phys. Chem. A*, 2010, **114**, 12155.
15 H. J. Zhai, J. C. Guo, S. D. Li and L. S. Wang, *ChemPhysChem*, 2011, **12**, 2549.
16 D. Z. Li, H. Bai, Q. Chen, H. G. Lu, H. J. Zhai and S. D. Li, *J. Chem. Phys.*, 2013, **138**, 244304.
17 H. J. Zhai, Q. Chen, H. Bai, H. G. Lu, W. L. Li, S. D. Li and L. S. Wang, *J. Chem. Phys.*, 2013, **139**, 174301.
18 W. J. Tian, H. G. Xu, X. Y. Kong, Q. Chen, W. J. Zheng, H. J. Zhai and S. D. Li, *Phys. Chem. Chem. Phys.*, 2014, **16**, 5129.
19 Q. Chen, H. G. Lu, H. J. Zhai and S. D. Li, *Phys. Chem. Chem. Phys.*, 2014, **16**, 7274.
20 D. Z. Li, L. J. Zhang, T. Ou, H. X. Zhang, L. Pei, H. J. Zhai and S. D. Li, *Phys. Chem. Chem. Phys.*, 2015, **17**, 16798.
21 W. J. Tian, L. J. Zhao, Q. Chen, T. Ou, H. G. Xu, W. J. Zheng, H. J. Zhai and S. D. Li, *J. Chem. Phys.*, 2015, **142**, 134305.
22 T. Ou, W. J. Tian, X. R. You, Y. J. Wang, K. Wang and H. J. Zhai, *Phys. Chem. Chem. Phys.*, 2015, **17**, 29697.
23 L. J. Zhao, W. J. Tian, T. Ou, H. G. Xu, G. Feng, X. L. Xu, H. J. Zhai, S. D. Li and W. J. Zheng, *J. Chem. Phys.*, 2016, **144**, 124301.
24 R. I. Kaiser and N. Balucani, *Acc. Chem. Res.*, 2017, **50**, 1154.
25 I. Boustani, *Int. J. Quantum Chem.*, 1994, **52**, 1081.
26 J. E. Fowler and J. M. Ugalde, *J. Phys. Chem. A*, 2000, **104**, 397.
27 J. I. Aihara, H. Kanno and T. Ishida, *J. Am. Chem. Soc.*, 2005, **127**, 13324.
28 J. M. Mercero, A. I. Boldyrev, G. Merino and J. M. Ugalde, *Chem. Soc. Rev.*, 2015, **44**, 6519.
29 E. Oger, N. R. M. Crawford, R. Kelting, P. Weis, M. M. Kappes and R. Ahlrichs, *Angew. Chem., Int. Ed.*, 2007, **46**, 8503.
30 H. J. Zhai, A. N. Alexandrova, K. A. Birch, A. I. Boldyrev and L. S. Wang, *Angew. Chem., Int. Ed.*, 2003, **42**, 6004.
31 H. J. Zhai, B. Kiran, J. Li and L. S. Wang, *Nat. Mater.*, 2003, **2**, 827.
32 A. P. Sergeeva, D. Y. Zubarev, H. J. Zhai, A. I. Boldyrev and L. S. Wang, *J. Am. Chem. Soc.*, 2008, **130**, 7244.
33 Y. J. Wang, Y. F. Zhao, W. L. Li, T. Jian, Q. Chen, X. R. You, T. Ou, X. Y. Zhao, H. J. Zhai, S. D. Li, J. Li and L. S. Wang, *J. Chem. Phys.*, 2016, **144**, 064307.
34 G. Martinez-Guajardo, A. P. Sergeeva, A. I. Boldyrev, T. Heine, J. M. Ugalde and G. Merino, *Chem. Commun.*, 2011, **47**, 6242.
35 J. O. C. Jiménez-Halla, R. Islas, T. Heine and G. Merino, *Angew. Chem., Int. Ed.*, 2010, **49**, 5668.
36 J. C. Guo, L. Y. Feng, Y. J. Wang, S. Jalife, A. Vasquez-Espinal, J. L. Cabellos, S. Pan, G. Merino and H. J. Zhai, *Angew. Chem., Int. Ed.*, 2017, **56**, 10174.
37 H. J. Zhai, Y. F. Zhao, W. L. Li, Q. Chen, H. Bai, H. S. Hu, Z. A. Piazza, W. J. Tian, H. G. Lu, Y. B. Wu, Y. W. Mu, G. F. Wei, Z. P. Liu, J. Li, S. D. Li and L. S. Wang, *Nat. Chem.*, 2014, **6**, 727.
38 G. L. Gutsev and A. I. Bolydrev, *Chem. Phys.*, 1981, **56**, 277.
39 G. L. Gutsev, C. A. Weatherford, L. E. Johnson and P. Jena, *J. Comput. Chem.*, 2012, **33**, 416.
40 S. R. Desai, H. Wu, C. M. Rohlfing and L. S. Wang, *J. Chem. Phys.*, 1997, **106**, 1309.
41 D. Y. Zubarev, A. I. Boldyrev, J. Li, H. J. Zhai and L. S. Wang, *J. Phys. Chem. A*, 2007, **111**, 1648.
42 S. Buckart, G. Ganteför, Y. D. Kim and P. Jena, *J. Am. Chem. Soc.*, 2003, **125**, 14205.
43 Y. Feng, H. G. Xu, Z. G. Zhang, Z. Gao and W. J. Zheng, *J. Chem. Phys.*, 2010, **132**, 074308.
44 Y. Feng, H. G. Xu, W. J. Zheng, H. M. Zhao, A. K. Kandalam and P. Jena, *J. Chem. Phys.*, 2011, **134**, 094309.
45 Y. Feng, G. L. Hou, H. G. Xu, Z. G. Zhang and W. J. Zheng, *Chem. Phys. Lett.*, 2012, **545**, 21.
46 P. Koirala, K. Pradhan, A. K. Kandalam and P. Jena, *J. Phys. Chem. A*, 2013, **117**, 1310.
47 H. Chen, X. Y. Kong, W. J. Zheng, J. N. Yao, A. K. Kandalam and P. Jena, *ChemPhysChem*, 2013, **14**, 3303.
48 X. Y. Kong, H. G. Xu, P. Koirala, W. J. Zheng, A. K. Kandalam and P. Jena, *Phys. Chem. Chem. Phys.*, 2014, **16**, 26067.
49 M. Willis, M. Götz, A. K. Kandalam, G. F. Ganteför and P. Jena, *Angew. Chem., Int. Ed.*, 2010, **49**, 8966.
50 H. G. Xu, Z. G. Zhang, Y. Feng, J. Y. Yuan, Y. C. Zhao and W. J. Zheng, *Chem. Phys. Lett.*, 2010, **487**, 204.
51 A. P. Sergeeva, B. B. Averkiev, H. J. Zhai, A. I. Boldyrev and L. S. Wang, *J. Chem. Phys.*, 2011, **134**, 224304.
52 M. Saunders, *J. Comput. Chem.*, 2004, **25**, 621.
53 P. P. Bera, K. W. Sattelmeyer, M. Saunders and P. v. R. Schleyer, *J. Phys. Chem. A*, 2006, **110**, 4287.

54 A. D. Becke, *J. Chem. Phys.*, 1993, **98**, 5648.
55 C. Lee, W. Yang and R. G. Parr, *Phys. Rev. B: Condens. Matter Mater. Phys.*, 1988, **37**, 785.
56 J. Čížek, *Adv. Chem. Phys.*, 1969, **14**, 35.
57 G. E. Scuseria and H. F. Schaefer III, *J. Chem. Phys.*, 1989, **90**, 3700.
58 R. J. Bartlett and M. Musial, *Rev. Mod. Phys.*, 2007, **79**, 291.
59 K. Raghavachari, G. W. Trucks, J. A. Pople and M. Head-Gordon, *Chem. Phys. Lett.*, 1989, **157**, 479.
60 M. E. Casida, C. Jamorski, K. C. Casida and D. R. Salahub, *J. Chem. Phys.*, 1998, **108**, 4439.
61 R. Bauernschmitt and R. Ahlrichs, *Chem. Phys. Lett.*, 1996, **256**, 454.
62 D. Y. Zubarev and A. I. Boldyrev, *Phys. Chem. Chem. Phys.*, 2008, **10**, 5207.
63 E. D. Glendening, J. K. Badenhoop, A. E. Reed, J. E. Carpenter, J. A. Bohmann, C. M. Morales and F. Weinhold, *NBO 5.0*, Theoretical Chemistry Institute, University of Wisconsin, Madison, 2001.
64 T. Lu and F. W. Chen, *Acta Chim. Sin.*, 2011, **69**, 2393.
65 M. J. Frisch, G. W. Trucks, H. B. Schlegel, G. E. Scuseria, M. A. Robb, J. R. Cheeseman, G. Scalmani, V. Barone, B. Mennucci, G. A. Petersson, H. Nakatsuji, M. Caricato, X. Li, H. P. Hratchian, A. F. Izmaylov, J. Bloino, G. Zheng, J. L. Sonnenberg, M. Hada, M. Ehara, K. Toyota, R. Fukuda, J. Hasegawa, M. Ishida, T. Nakajima, Y. Honda, O. Kitao, H. Nakai, T. Vreven, J. A. Montgomery, Jr., J. E. Peralta, F. Ogliaro, M. Bearpark, J. J. Heyd, E. Brothers, K. N. Kudin, V. N. Staroverov, R. Kobayashi, J. Normand, K. Raghavachari, A. Rendell, J. C. Burant, S. S. Iyengar, J. Tomasi, M. Cossi, N. Rega, J. M. Millam, M. Klene, J. E. Knox, J. B. Cross, V. Bakken, C. Adamo, J. Jaramillo, R. Gomperts, R. E. Stratmann, O. Yazyev, A. J. Austin, R. Cammi, C. Pomelli, J. W. Ochterski, R. L. Martin, K. Morokuma, V. G. Zakrzewski, G. A. Voth, P. Salvador, J. J. Dannenberg, S. Dapprich, A. D. Daniels, Ö. Farkas, J. B. Foresman, J. V. Ortiz, J. Cioslowski and D. J. Fox, *Gaussian 09, Revision D.01*, Gaussian, Inc., Wallingford, CT, 2009.
66 P. Pyykkö and M. Atsumi, *Chem. – Eur. J.*, 2009, **15**, 12770.
67 While isomer **3c** ranks the third at B3LYP level, it becomes slightly higher than **3d** at single-point CCSD(T) (Fig. S3, ESI†). Thus **3a**, **3b**, and **3d** are three ultimately lowest-energy isomers of $Al_3BO_2^-$. Since both **3a** and **3d** are observed in the PE spectra (Fig. 2), **3b** is anticipated to be present experimentally as well. In fact, the PE spectra exhibit continuous weak signals in the 1.5–2.0 eV regime (Fig. 2), to which isomer **3b** should contribute.
68 AdNDP[62] is an extension of NBO analysis and represents the bonding of a molecule in terms of *n*-center two-electron (*n*c–2e) bonds, with *n* ranging from one to the total number of atoms in the system. Thus AdNDP recovers not only classical Lewis elements (lone pairs and 2c–2e bonds), but also delocalized *n*c–2e bonds.